

NO-A178 490

DETERMINATION OF THE BEST HYDRODYNAMIC PARAMETER FOR  
MODELLING FLOW ON CA. (U) DAVID W TAYLOR NAVAL SHIP  
RESEARCH AND DEVELOPMENT CENTER ANN. R GUANTI ET AL.  
DEC 86 DTNSRDC/SNE-86-78 F/G 11/3

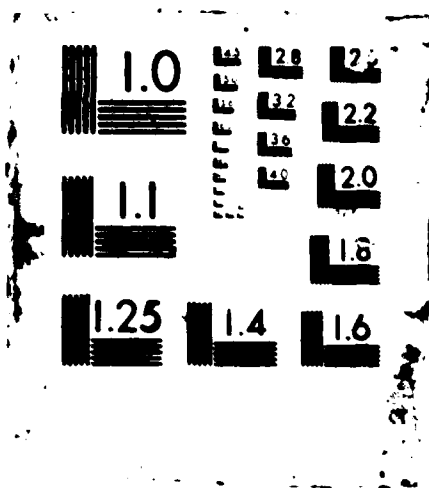
1/1

**UNCLASSIFIED**

**F/G 11/3**

NL

Figure 1 displays a sequence of 39 grayscale images arranged in a 3x13 grid. The images show the progression of a handwritten digit '1' from left to right. The first image on the left is very faint and noisy. As the images progress, the digit becomes increasingly clear and defined. The final image on the right shows a very clear, high-contrast digit '1'.



2

# David W. Taylor Naval Ship Research and Development Center

Bethesda, MD 20084-5000

DTIC FILE COPY

DTNSRDC/SME-86-78

Ship Materials Engineering Department  
Research and Development Report

DETERMINATION OF THE BEST HYDRODYNAMIC PARAMETER FOR  
MODELLING FLOW ON CATHODICALLY POLARIZED SURFACES

by

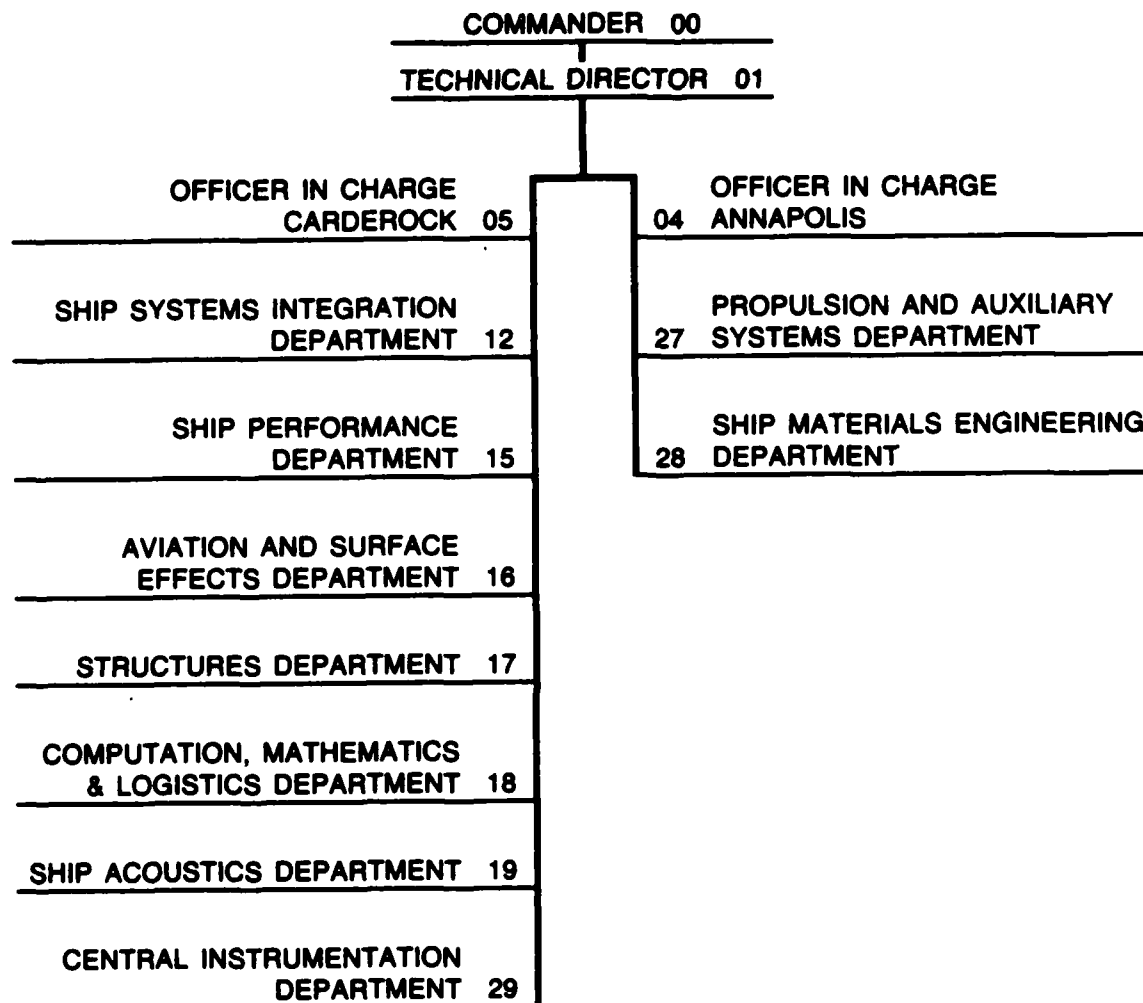
Robert Guanti and Harvey Hack

DTIC  
ELECTE  
APR 03 1987  
S  
D  
D

Approved for public release; distribution unlimited.



## MAJOR DTNSRDC TECHNICAL COMPONENTS



UNCLASSIFIED

SECURITY CLASSIFICATION OF THIS PAGE

## REPORT DOCUMENTATION PAGE

1a. REPORT SECURITY CLASSIFICATION <b>UNCLASSIFIED</b>		1b. RESTRICTIVE MARKINGS <b>A178 490</b>	
2a. SECURITY CLASSIFICATION AUTHORITY		3. DISTRIBUTION/AVAILABILITY OF REPORT Approved for public release; distribution unlimited.	
2b. DECLASSIFICATION/DOWNGRADING SCHEDULE			
4. PERFORMING ORGANIZATION REPORT NUMBER(S) <b>DTNSRDC/SME-86-78</b>		5. MONITORING ORGANIZATION REPORT NUMBER(S) <b>1</b>	
6a. NAME OF PERFORMING ORGANIZATION <b>David W. Taylor Naval Ship R&amp;D Center</b>	6b. OFFICE SYMBOL (If applicable) <b>Code 2813</b>	7a. NAME OF MONITORING ORGANIZATION	
6c. ADDRESS (City, State, and ZIP Code) <b>Bethesda, MD 20084-5000</b>		7b. ADDRESS (City, State, and ZIP Code)	
8a. NAME OF FUNDING/SPONSORING ORGANIZATION	8b. OFFICE SYMBOL (If applicable)	9. PROCUREMENT INSTRUMENT IDENTIFICATION NUMBER	
8c. ADDRESS (City, State, and ZIP Code)		10. SOURCE OF FUNDING NUMBERS	
		PROGRAM ELEMENT NO <b>63561N</b>	PROJECT NO <b>001</b>
		TASK NO. <b>S1266-</b> <b>001</b>	WORK UNIT ACCESSION NO <b>1508-004-71</b>
11. TITLE (Include Security Classification) <b>DETERMINATION OF THE BEST HYDRODYNAMIC PARAMETER FOR MODELLING FLOW ON CATHODICALLY POLARIZED SURFACES</b>			
12. PERSONAL AUTHOR(S) <b>Robert Guanti and Harvey Hack</b>			
13a. TYPE OF REPORT	13b. TIME COVERED FROM TO	14. DATE OF REPORT (Year, Month, Day) <b>December 1986</b>	15. PAGE COUNT <b>34</b>
16. SUPPLEMENTARY NOTATION			
17. COSATI CODES		18. SUBJECT TERMS (Continue on reverse if necessary and identify by block number)	
FIELD	GROUP	SUB-GROUP	
		Velocity experiments	
		Polarization curves	
		Rotating cylinder electrode	
		Potentiostatic tests	
		Flow conditions	
19. ABSTRACT (Continue on reverse if necessary and identify by block number)			
<p>Short and long term velocity experiments were performed utilizing a rotating cylinder electrode. This was to determine the best way to model in the laboratory the flow conditions in service on a cathodically polarized surface or on anodically polarized zinc. This was studied by measuring the cathodic current required to protect HY-80 steel, nickel-aluminum-bronze and commercially pure titanium in flowing seawater. Potentiodynamic scans on a one inch diameter cylindrical specimen were run at rotation speeds of 50, 100, 200, 800 and 2000 rpm. The limiting current portion of the resulting polarization curves indicated that all three materials illustrated rotation speed dependent behavior. This behavior was consistent with a mechanism whereby the reaction kinetics are governed by oxygen diffusion through a fluid boundary layer. The currents measured for HY-80 were approximately an order of magnitude lower than those consistent with boundary layer diffusion, due to the formation of a barrier layer of calcareous deposits or fouling. Increased</p> <p>(Continued)</p>			
20. DISTRIBUTION/AVAILABILITY OF ABSTRACT <input type="checkbox"/> UNCLASSIFIED/UNLIMITED <input type="checkbox"/> SAME AS RPT <input type="checkbox"/> DTIC USERS		21. ABSTRACT SECURITY CLASSIFICATION <b>UNCLASSIFIED</b>	
22a. NAME OF RESPONSIBLE INDIVIDUAL <b>Harvey Hack</b>		22b. TELEPHONE (Include Area Code) <b>(301) 267-3754</b>	22c. OFFICE SYMBOL <b>Code 2813</b>

## Block 19 (Continued)

rotation speeds, which result in increased shear stresses resulted in currents more consistent with the diffusion model, indicating that higher velocities result in stripping away surface deposits or change the morphology of the barrier film.

The effect of velocity on the anodic current output for zinc sacrificial anodes was also evaluated to determine the best way to model flow over a sacrificial anode. Some velocity effects were observed, but could not be related to a specific reaction control mechanism.

Long term potentiostatic tests were run to determine the effect of corrosion products and/or biological films on flow modelling of cathodic current demand. Rotation speeds of 40, 160, 800, 1600 and 2000 rpm were studied. The initial currents observed for bronze and steel correlated well with those values predicted for boundary layer diffusion. Shortly after polarizing these materials, the cathodic current decreased more than an order of magnitude, probably due to the formation of a film, such as a calcareous deposit. Titanium illustrated low currents initially, possibly due to the presence of a surface film. After a brief period of cathodic protection the current increased, indicating that the initial film was reduced. Upon reaching steady state the currents were still lower than for boundary layer diffusion, indicating the presence of another film.

# CONTENTS

	Page
ABSTRACT.....	1
ADMINISTRATIVE INFORMATION.....	1
INTRODUCTION.....	2
MATERIALS.....	4
APPARATUS.....	5
EXPERIMENTAL PROCEDURE.....	6
RESULTS AND DISCUSSION.....	6
SUMMARY AND CONCLUSIONS.....	11
REFERENCES.....	27

## FIGURES

1. Schematic representation of rotating cylinder electrode set-up.....	12
2. Rotating cylinder electrode specimen holder.....	13
3. Potentiodynamic scans of nickel-aluminum-bronze at 50, 100, 200, 800 and 2000 rpm.....	14
4. Potentiodynamic scans of HY 80 steel at 50, 100, 200, 800 and 2000 rpm.....	15
5. Potentiodynamic scans of CP titanium at 50, 100, 200, 800 and 2000 rpm.....	16
6. Potentiodynamic scans of zinc anode materials at 50, 100, 200, 800 and 2000 rpm.....	17
7. Plots of polarization curves of zinc anode materials as a function of overpotential.....	18



Availability Codes	
Dist	Avail and/or Special
A-1	

## FIGURES (Continued)

	Page
8. Comparison of predicted versus observed currents measured by the rotating cyclinder electrode apparatus for nickel-aluminum-bronze, CP titanium and HY 80 steel.....	19
9. Normalized polarization curves for nickel-aluminum-bronze.....	20
10. Normalized polarization curves for CP titanium.....	21
11. Normalized polarization curves for HY 80 steel.....	22
12. Long term potentiostatic curves of nickel-aluminum-bronze at 40, 160, 800, 1600 and 2000 rpm.....	23
13. Long term potentiostatic curves of CP titanium at 40, 160, 800, 1600 and 2000 rpm.....	24
14. Long term potentiostatic curves of HY 80 at 40, 160, 800, 1600 and 2000 rpm.....	25

## TABLE

1. Percent Composition of Alloys Tested.....	4
--	---



# SYMBOLS

- CP - Commercially Pure
- $\delta$  - Nernst Diffusion Layer Thickness (cm)
- D - Diffusivity of Reacting Species ( $\text{cm}^2 \text{sec}^{-1}$ )
- V - Velocity ( $\text{cm sec}^{-1}$ )
- $d_1$  - Diameter of Rotating Electrode (cm)
- $\nu$  - Kinematic Viscosity of Seawater ( $\text{cm}^2 \text{sec}^{-1}$ )
- $i_L$  - Limiting Current Density ( $\text{A cm}^{-2}$ )
- n - Equivalent per Mole
- F - Faraday's Constant (coulomb)
- $C_0$  - Bulk Concentration of Reacting Species ( $\text{mole cc}^{-1}$ )
- $\tau$  - Shear Stress ( $\text{g cm}^{-1} \text{sec}^{-2}$ )
- f - Friction Factor (dimensionless)
- $\rho$  - Density ( $\text{g cm}^{-3}$ )
- $\omega$  - Angular Velocity ( $\text{radians sec}^{-1}$ )
- Re - Reynolds Number =  $Vd_1\nu^{-1}$  (dimensionless)
- rpm - Revolutions per minute

## ABSTRACT

Short and long term velocity experiments were performed utilizing a rotating cylinder electrode. This was to determine the best way to model in the laboratory the flow conditions in service on a cathodically polarized surface or on anodically polarized zinc. This was studied by measuring the cathodic current required to protect HY-80 steel, nickel-aluminum-bronze and commercially pure titanium in flowing seawater. Potentiodynamic scans on a one inch diameter cylindrical specimen were run at rotation speeds of 50, 100, 200, 800 and 2000 rpm. The limiting current portion of the resulting polarization curves indicated that all three materials illustrated rotation speed dependent behavior. This behavior was consistent with a mechanism whereby the reaction kinetics are governed by oxygen diffusion through a fluid boundary layer. The currents measured for HY-80 were approximately an order of magnitude lower than those consistent with boundary layer diffusion, due to the formation of a barrier layer of calcareous deposits or fouling. Increased rotation speeds, which result in increased shear stresses resulted in currents more consistent with the diffusion model, indicating that higher velocities result in stripping away surface deposits or change the morphology of the barrier film.

The effect of velocity on the anodic current output for zinc sacrificial anodes was also evaluated to determine the best way to model flow over a sacrificial anode. Some velocity effects were observed, but could not be related to a specific reaction control mechanism.

Long term potentiostatic tests were run to determine the effect of corrosion products and/or biological films on flow modeling of cathodic current demand. Rotation speeds of 40, 160, 800, 1600 and 2000 rpm were studied. The initial currents observed for bronze and steel correlated well with those values predicted for boundary layer diffusion. Shortly after polarizing these materials, the cathodic current decreased more than an order of magnitude, probably due to the formation of a film, such as a calcareous deposit. Titanium illustrated low currents initially, possibly due to the presence of a surface film. After a brief period of cathodic protection the current increased, indicating that the initial film was reduced. Upon reaching steady state the currents were still lower than for boundary layer diffusion, indicating the presence of another film.

## ADMINISTRATIVE INFORMATION

The work described herein was performed under Work Unit 1-1508-004-71 under NAVSEA SSN 21 propulsor task program element 63561N task area S1266001. The task leader is Mr. F. Lengenfelder and DTNSRDC Project manager is Mr. Bob

Boswell. The work was conducted in the Marine Corrosion Branch under the supervision of Mr. A.G.S. Morton.

## INTRODUCTION

Design criteria for cathodic protection for structures exposed to quiescent seawater are well documented. Determining the cathodic current demand for protecting a structure in flowing seawater becomes more difficult due to the unknown effect of flow. Reproducing service flow conditions in the laboratory involves knowledge of the flow parameter that best determines the cathodic current density at various flow rates. At present the best parameter to use for flow modelling is unknown. This study is the first attempt to determine the best hydrodynamic parameter for flow modelling.

The principal reaction that can occur on a cathodically protected structure is oxygen reduction, which is highly dependent on mass transport of dissolved oxygen to the surface, where it reacts to form hydroxyl ions. These ions can locally shift the pH enough to decrease the amount of calcium and magnesium compounds which can be held in solution, thus precipitating out a calcareous deposit on the surface. Hydrogen evolution can also occur to a significant extent, depending on overpotential and pH. On sacrificial anodes the principal anodic reaction is metal dissolution, which may be under activation control, but could also under some conditions be under control by mass transport of metal ions away from the surface.

Any of these transport-controlled reactions can be limited by diffusion of the products or reactants through a fluid boundary layer such as the Nernst diffusion layer, or by diffusion through a corrosion product, calcareous film, or fouling layer on the surface. In addition, transition to activation control can occur if the catalysis rate of the controlling reaction is extremely low on the corrosion product or calcareous deposit.

In this study, alloys were polarized potentiostatically to potentials which support primarily oxygen reduction. Since this reaction is dependent on oxygen transport to the cathode surface, its rate can be affected by the hydrodynamic boundary layer thickness, which is related to the Nernst diffusion layer thicknesses, or by the presence of calcareous and corrosion product film formations which provide an oxygen diffusion barrier. In the former case, the current required for the cathodic reaction will depend on some measure of the hydrodynamic or diffusion boundary layer thickness, whereas in the latter case the current will be fairly constant with increasing flow until some critical shear stress is reached at the surface which strips off the current-limiting films.

One approach to determining the cathodic current requirement is to model the diffusion layer thickness or shear stress at the surface by utilizing a rotating cylinder electrode, since the hydrodynamic conditions established by this apparatus are well defined. The Nernst diffusion layer thickness, ( $\delta$ ), in this apparatus is a function of velocity and can be calculated from the following equation:

$$\delta = 12.64 D/V (Vd_1/v)^{0.30} (v/D)^{0.644}$$

which was derived from groups of dimensionless numbers determined by Eisenberg et al<sup>1</sup>, and assumes uniform current distribution and turbulent flow. The theoretical maximum cathodic current can then be calculated from:

$$i_L = n F D C_0 / \delta$$

to give:

$$i_L = 0.079 n F C_0 V (Vd_1/v)^{-0.30} (v/D)^{-0.644}$$

The shear stress on the surface of the rotating electrode can be

calculated from the following equation<sup>1</sup>:

$$\tau = f/2 \rho w^2 r_i^2$$

where the friction factor (f) is defined for a smooth cylinder as follows:

$$\frac{f}{2} = 0.079 \text{ Re}^{-0.30}$$

Although the hydrodynamics of this device are well defined when operating in turbulent flow, it is important to ascertain that the correlation between experimental and theoretical mass transport parameters are maintained for the actual apparatus used. The validity of the set-up can be evaluated by comparing theoretical and experimental Nusselt or Sherwood Numbers, known as the Eisenberg Correlation,<sup>1</sup> or to compare theoretical and experimental limiting current values, as is done in this study.

#### MATERIALS

The materials tested included HY-80 steel, nickel-aluminum bronze, commercially pure titanium, and anode grade zinc (MIL-SPEC-18001J).

The chemical compositions of these materials are listed in Table 1.

Table 1. Percent Composition of Alloys Tested

Elements	Alloys			
	HY-80	Ni-Al-Br	Ti	Zn Anode
Iron	REM	3.93	0.83	0.0090
Copper	-	80.1	-	0.0020
Nickel	2.49	4.66	-	<0.0005
Zinc	-	0.44	-	99.8
Aluminum	-	9.44	-	0.166
Cadmium	-	-	-	0.411
Manganese	0.30	1.55	-	-
Carbon	0.132	-	0.017	-
Silicon	0.20	0.092	-	-
Sulfur	0.017	-	-	-
Tin	-	0.077	-	-
Cobalt	-	0.014	-	-
Chromium	1.72	0.007	-	-
Molybdenum	0.41	-	-	-
Phosphorus	0.011	-	-	-
Nitrogen	-	-	0.007	-
Hydrogen	-	-	0.003	-
Oxygen	-	-	0.077	-

## APPARATUS

The apparatus, shown in Fig. 1 was a rotating cylinder electrode in a specially-constructed test cell. The electrolyte used was natural seawater, which was heated and aerated in a separate reservoir prior to its introduction into the test cell. The temperature of the seawater was monitored daily and maintained at  $30^{\circ}\text{C} \pm 3$  with an immersion heater in the makeup water reservoir. The cell walls were composed of 1/4" Plexiglass having dimensions of 6 inches in diameter by 6 inches in height.

The rotator was a Pine Instrument Company model AFASR, which has a rotation speed range of 50 to 10000 rpm. The specimen holder consisted of a specially machined titanium rod, tapered on one end and with 1/2" - 20 (class 3) threads on the other (see Fig. 2). Electrical contact to the specimen was made through the rotor and a carbon brush contact. The test specimen was a 1 inch diameter cylinder threaded on the inside and 1 inch in height. In preparation for testing the specimen was inserted between two threaded roulon spacers fitted with o-ring seals to prevent crevice attack and to avoid seawater contacting the titanium rotor. The counter electrode was made from platinized screen 5.5 inches in diameter and 0.5 inch in height and was positioned concentrically to the test specimen.

Potentiodynamic scans utilized a variety of potentiostats, including E G and G PAR models 173 and 350A, and a Petrolyte Potentiodyne Analyzer. Long term potentiostatic tests utilized a multichannel potentiostat Model 440 designed by Scriber Associates Inc. For the long-term exposures, specimen currents and potentials were monitored and recorded on a computerized data acquisition system described previously.<sup>2</sup>

## EXPERIMENTAL PROCEDURE

Potentiodynamic scans were conducted on all materials at rotation speeds of 50, 100, 200, 800, and 2000 rpm. All materials except zinc were first held potentiostatically at -1300 mV versus SCE for ten minutes to allow current stabilization before beginning a scan to the corrosion potential using a scan rate of 0.1 mV/s. Zinc scans were initiated at the corrosion potential ten minutes after exposure and proceeded in the noble direction at the same scan rate.

Long term (30 days) exposures were also run to determine the effect of calcareous product buildup on cathodic current densities. Specimens of each material were controlled potentiostatically at -800 millivolts versus SCE (except zinc, where a potential of -1030 mV was used) and the current and potential were monitored. Rotation speeds used were 40, 160, 800, 1600, and 2000 rpm.

## RESULTS AND DISCUSSION

Figures 3 through 6 illustrate the results of the potentiodynamic exposures. The bronze in Fig. 3 shows no significant effect of rotation speed on corrosion potential. The hydrogen evolution reaction is observed below -1100 mV and has a rotation-speed-independent location. The slope is also rotation speed independent and ranged from 120 to 135 mV per decade. The vertical portions of the curves have increasing current densities with increasing rotation speed. A Tafel-like region is observed just negative to the corrosion potential, which becomes almost exactly vertical at more negative potentials. This behavior is consistent with a model where the reaction rate is under mass transport control by diffusion through a Nernst boundary layer.

The HY-80 steel in Fig. 4 exhibits some positive shift in corrosion potential with increasing rotation speed. Like the bronze, a speed-independent hydrogen evolution line of slope 120 mV per decade is observed, although the location of this line is somewhat different from the bronze. The steel exhibits no Tafel-like behavior, but transitions directly from the corrosion potential to a somewhat vertical, rotation-speed-dependent behavior until the hydrogen evolution reaction is reached.

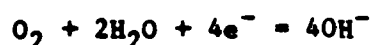
The titanium in Fig. 5 shows a major positive shift in corrosion potential with increasing rotation speed, a Tafel-like behavior below the corrosion potential, and a vertical, rotation-dependent behavior at more negative potentials. The slight deviation of the 200 rpm curve from this pattern is due to experimental error. The absence of the hydrogen evolution line is due to the low exchange current density for hydrogen generation on Ti ( $i_0 = 10^{-8.2}$  amp/cm<sup>2</sup>)<sup>3</sup>, meaning that this material is a poor electrocatalyst for the hydrogen evolution reaction. Although the  $i_0$  referred to above was determined in an acid medium, laboratory tests utilizing ASTM and natural seawater illustrated similar results ( $10^{-8}$  amp/cm<sup>2</sup>). With this low exchange current density, the hydrogen line would not be expected to be visible above -1300 mV.

Anodic curves for zinc shown in Fig. 6 are difficult to interpret relative to flow dependence. Two different zinc specimens were used for these tests, and the two observed corrosion potentials are likely to be due to a inhomogeneity in the zinc material which led to different potentials for the different specimens. In Fig. 7, the zinc curves are plotted as a function of overpotential. Between 0 and 50 mV overpotential, zinc shows a systematic current increase with increasing rotation speed. Above 50 mV overpotential the effect of rotation speed becomes insignificant. The anodic corrosion of zinc is usually thought to be activation controlled which would result in rotation speed independence.



One explanation for the observed rotation speed dependence is the presence of an air-formed barrier oxide which is more rapidly removed under high flow conditions. In this case, the rotation speed dependence should disappear with increasing exposure duration as the zinc undergoes anodic dissolution and this oxide is removed.

To ascertain whether the rotating cylinder apparatus was operating in the proper hydrodynamic regime, experiments were conducted to confirm that correlation was maintained between theoretical and experimentally determined limiting current values. This approach requires that the specimen be polarized to the limiting current regime of the controlling reaction (in this case oxygen reduction):



at which time the concentration of reacting species at the electrode surface approaches zero and the theoretical value of the limiting current can be calculated. To determine the potential range at which the current becomes limited at different rotation speeds, results from the potentiodynamic scans were used.

After determining the limiting current potential range for the different velocities, a potential which intersected this regime for all rotation speeds was selected. This potential was -800 mV versus SCE. Specimens were polarized to this potential until the current stabilized during rotation at 2000 rpm. This took 10 minutes to several hours. Rotation speed was then stepped down in 10-minute increments to 1600, 800, 400, 200, 100, and finally, 50 rpm. The stable current value was recorded for each speed. Plots were then made of the experimental vs. the theoretical limiting current values, calculated from the following equation:

$$i_L = 0.079 \ln FC_0 (Vd_1/v)^{-0.30} (v/D)^{-0.644}$$

The degree of fit between the data and the theory is shown in Fig. 8 and confirms the accuracy of the hydrodynamics of the apparatus. Good correlation was maintained throughout the velocity range evaluated with the greatest deviation being approximately 12% for bronze at 2000 rpm. To determine whether the reaction kinetics in the rotation-speed dependent areas of the curves were governed by the diffusion rate of oxygen through the fluid boundary layer, the cathodic potentiodynamic data were treated as follows. If the current is limited by diffusion through the Nernst boundary layer, this current should vary as rotation speed to the 0.7 power. Thus if the current at each rotation speed is divided by that speed to the 0.7 power, those areas of the curves which are controlled by boundary-layer diffusion should become co-incident. This was done for the cathodic curves in Figs. 9 through 11. Bronze and titanium showed good co-incidence of the curves in the areas which were rotation-speed dependent, particularly in the more negative parts of the curves, indicating boundary-layer diffusion control and implying that no additional surface films were present to slow oxygen diffusion. The theoretical value for the coincidence point is 28.14, which corresponds well with the observed values. The steel data showed approximately an order of magnitude deviation from co-incidence, with the normalized currents increasing with rotation speed. Since all of the experimental values are lower than the predicted value of 28.14, the specimens must have formed a surface film, possibly calcareous, which limited the rate of oxygen diffusion above that of the Nernst layer. Increasing speed slowed development of this film or generated more shear force to strip it off, allowing the higher rotation speed data to more closely approximate ideal Nernst layer diffusion.

Long term potentiostatic test results are presented as current versus time plots in Figs. 12 through 14. Bronze and steel initially displayed currents equivalent to those predicted from Nernst layer diffusion, followed by a decrease before stabilizing. The steel data shows less scatter than the bronze and converges to a speed-independent value. Scatter is too great for the bronze data to determine if the final value is speed-independent. In both cases the reason for the decrease in current is likely due to fouling or calcareous deposits forming on the surface of the electrode. After testing, fouling was observed on specimens for all rotation speeds and calcareous deposits were present for all velocities except 2000 rpm. The scatter observed for bronze indicates that this material does not form as tenacious a film as the steel or that the film that is formed is unique for each substrate. The increased tenacity of the film on steel is in support of the potentiodynamic data, where steel was the only material to have a barrier film in the short-term test.

The low currents observed for Ti at the beginning of the test runs indicate that a surface oxide was present on the specimen prior to starting the test. Shortly after applying the cathodic potentials the current increased due to the surface film being reduced. Stable current values were still below those predicted from Nernst layer diffusion, indicating the presence of an additional oxygen barrier, such as a calcareous deposit. After testing, the only specimen that contained visible calcareous deposits was the sample rotated at 40 rpm. The other specimens appeared shiny and free of surface films. However, the lower than predicted currents imply that an oxide or film must have been present.

## SUMMARY AND CONCLUSIONS

The data for bronze, titanium, and steel are consistent with a mechanism whereby cathodic protection current is initially controlled by oxygen diffusion through a fluid boundary layer, after first reducing an air-formed film on the titanium. After longer periods of exposure, the buildup of a layer of calcareous deposits and fouling results in considerable reduction of the current density required for cathodic protection. Thus for short-term exposures of these materials at cathodic overpotentials, flow effects can be modelled by duplicating the diffusion boundary layer thickness of that in service. For longer term exposures, the buildup of a current-limiting deposit may eventually lead to velocity-independent current densities, providing that the shear stress at the surface is below that for removal of this barrier deposit.

Anodic polarization of zinc anode material is initially flow-dependent by a mechanism as yet undefined. Therefore, no conclusions can yet be made about the best method for modelling flow across a zinc anode.

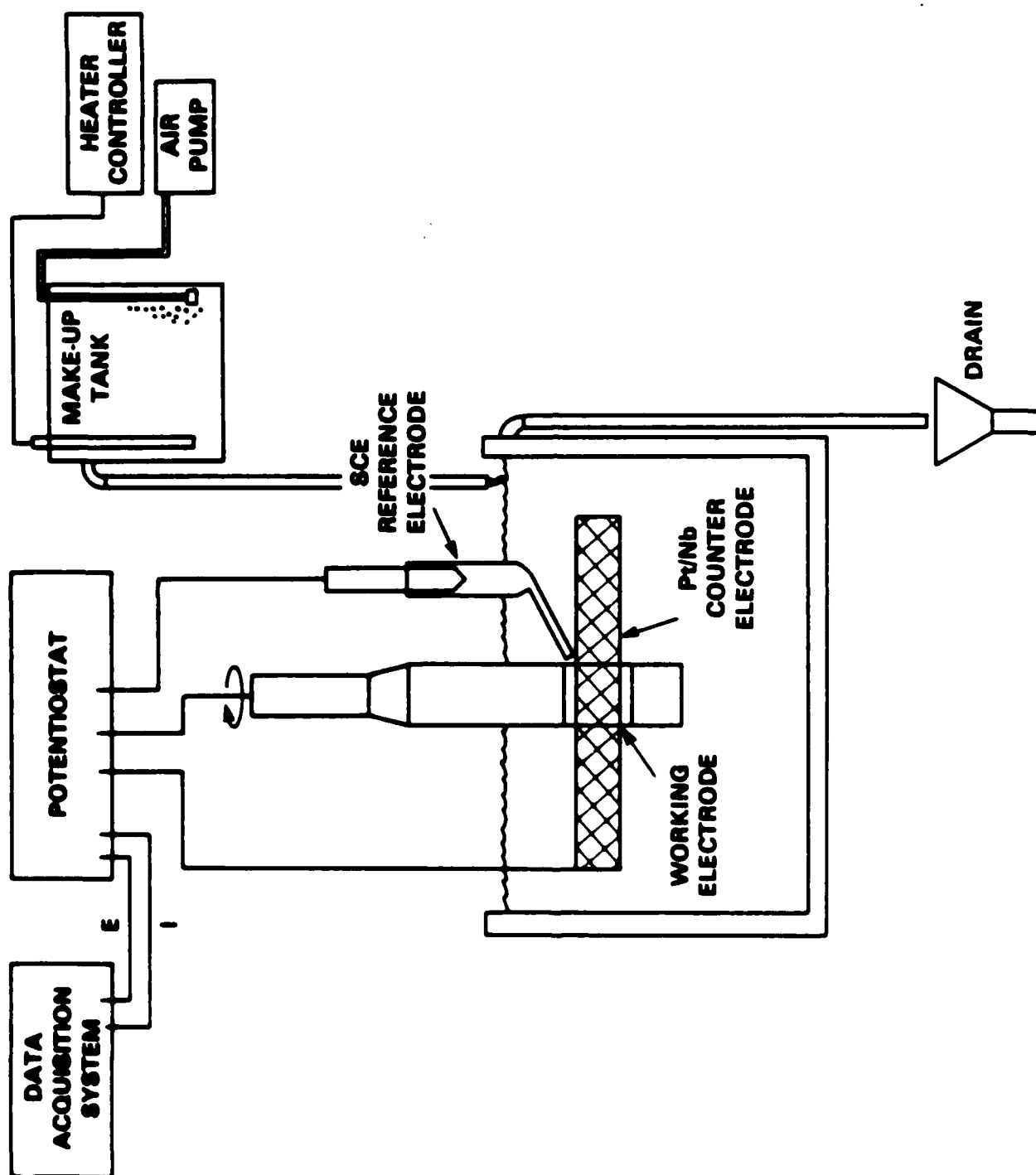


Fig. 1. Schematic representation of rotating cylinder electrode set-up.

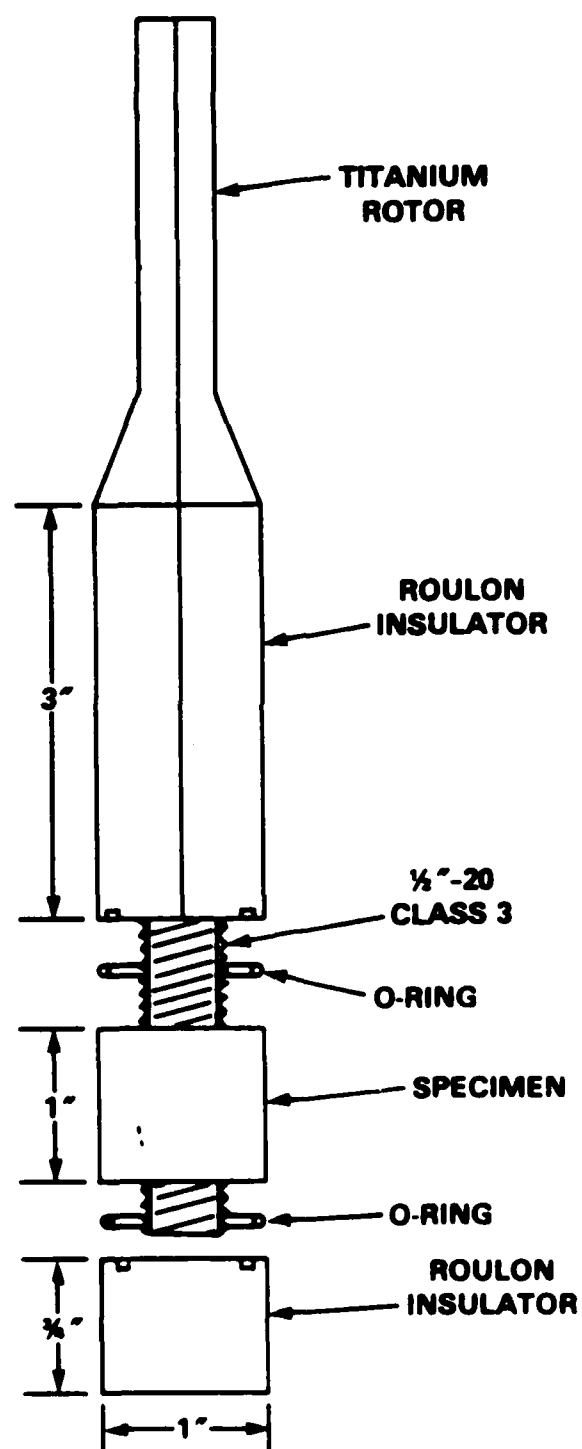


Fig. 2. Rotating cylinder electrode specimen holder.

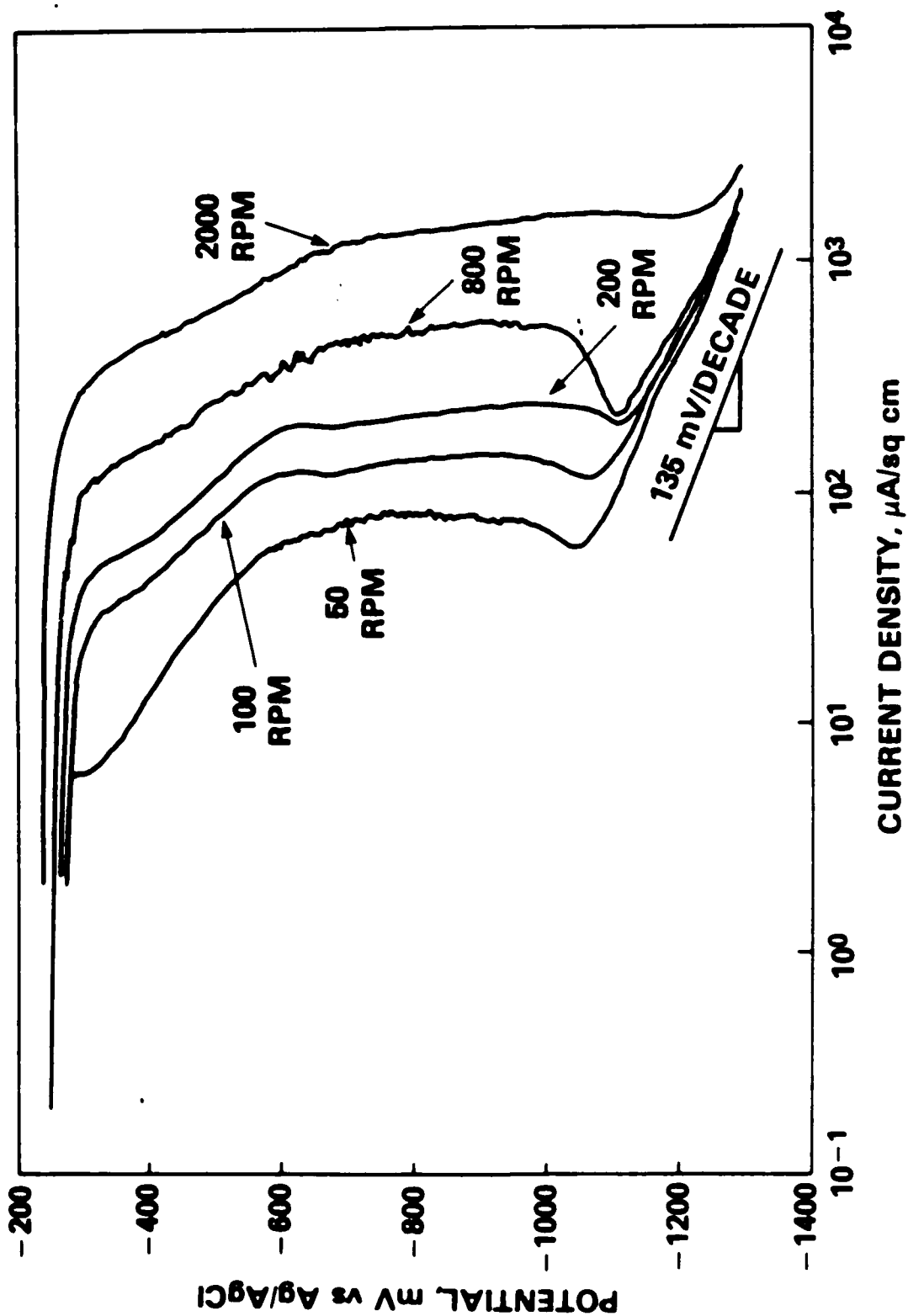


Fig. 3. Potentiodynamic scans of nickel-aluminum-bronze at 50, 100, 200, 800 and 2000 rpm.

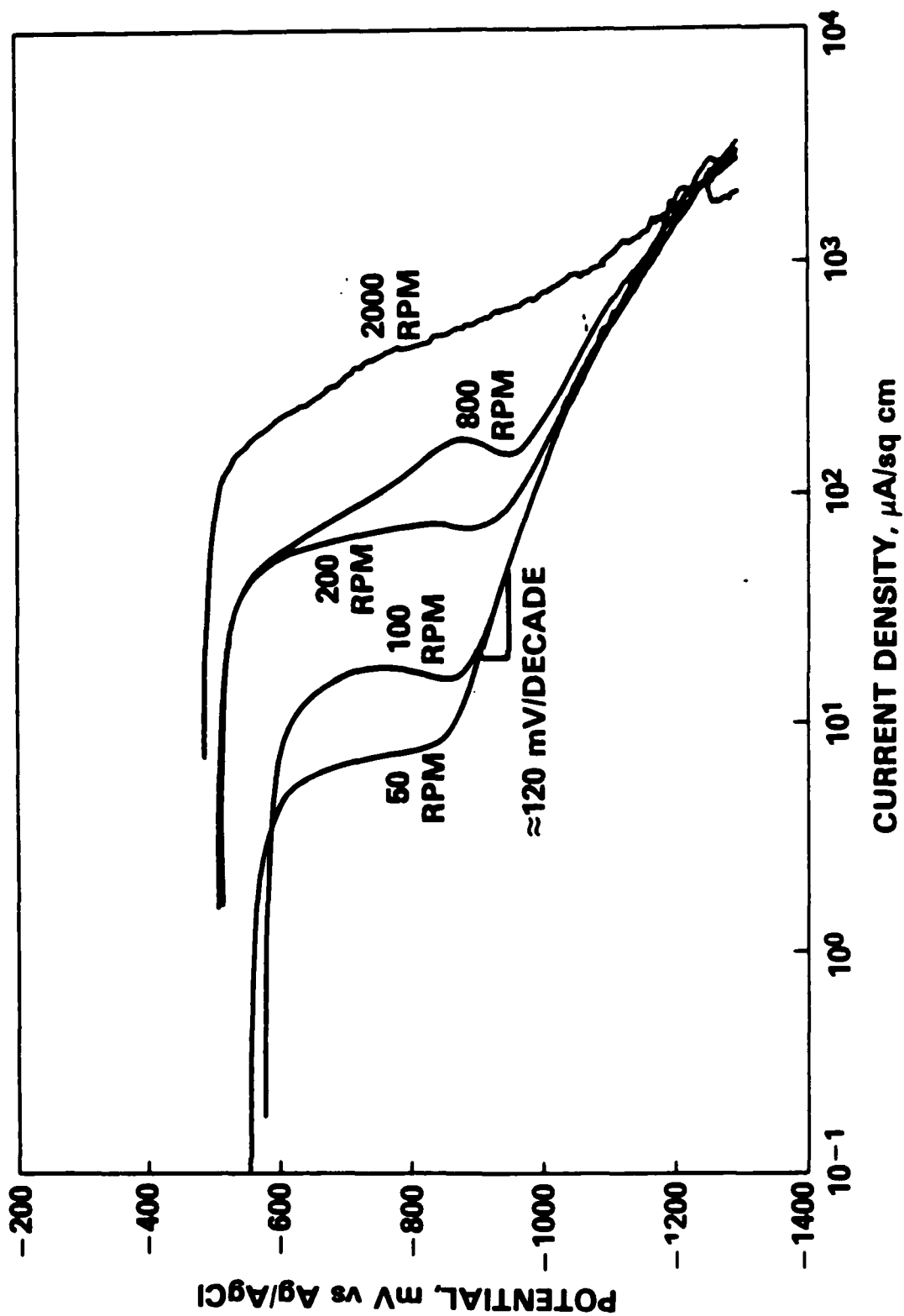


Fig. 4. Potentiodynamic scans of HY 80 steel at 50, 100, 200, 800 and 2000 rpm.



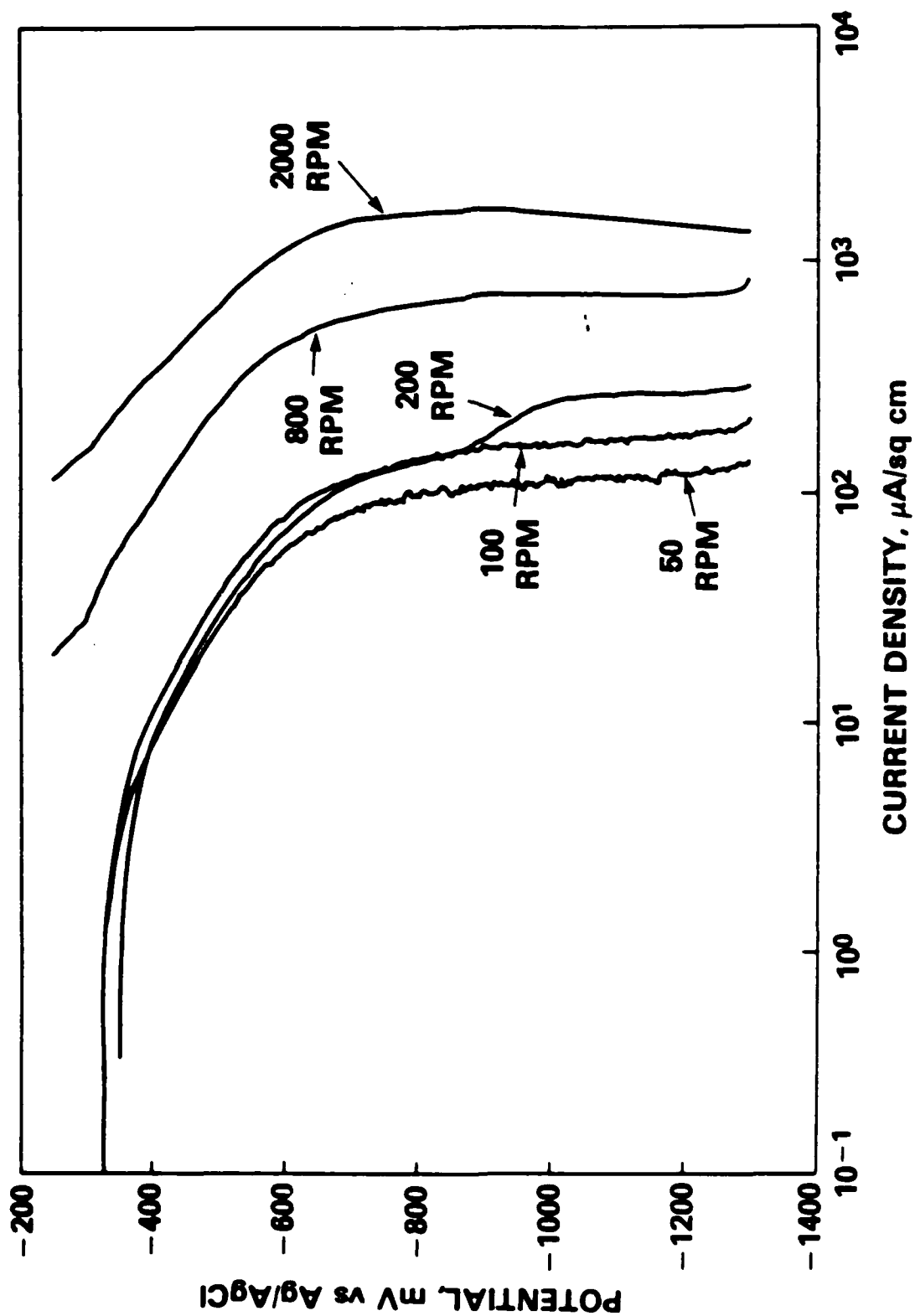


Fig. 5. Potentiodynamic scans of CP titanium at 50, 100, 200, 800 and 2000 rpm.

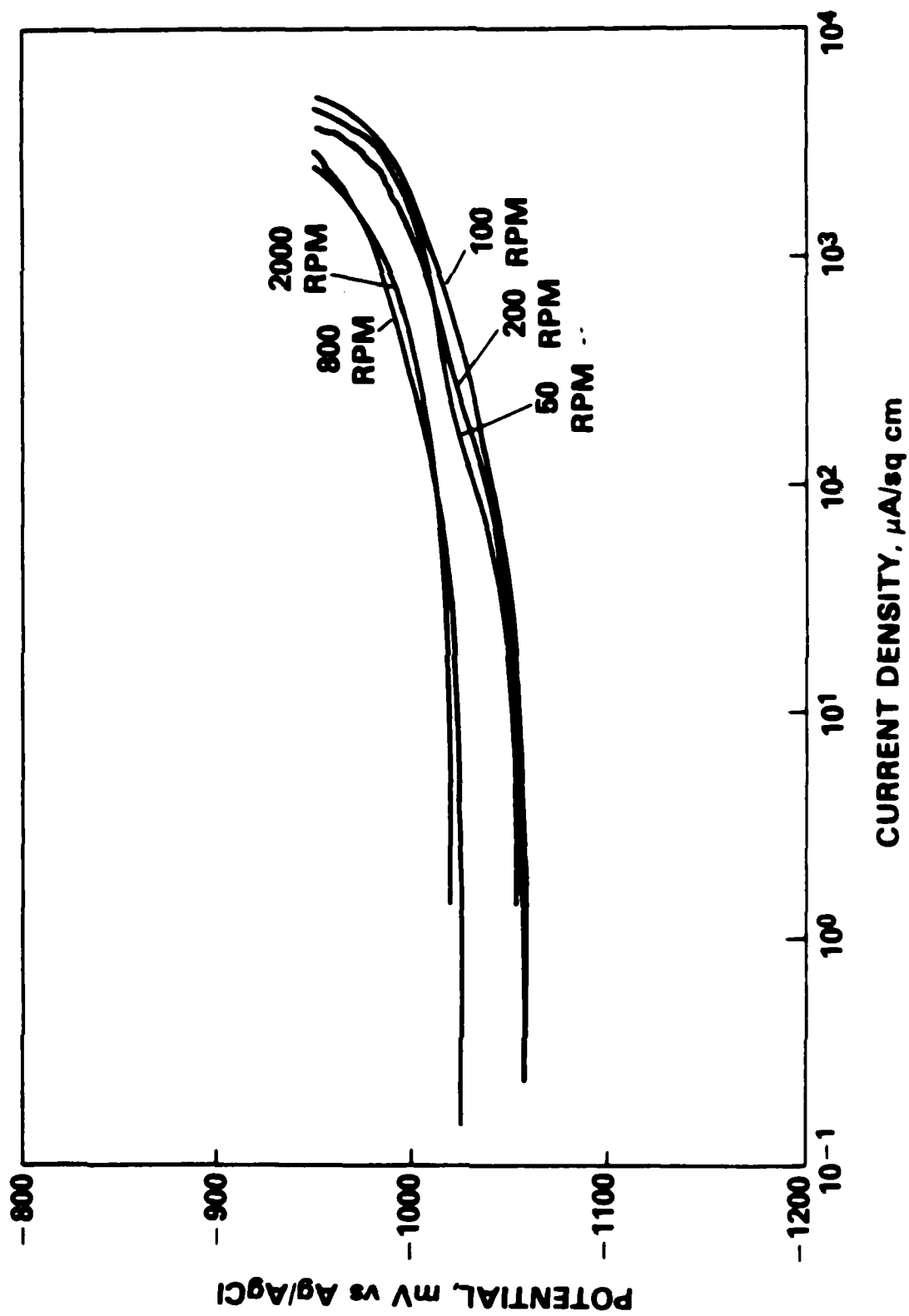


Fig. 6. Potentiodynamic scans of zinc anode materials at 50, 100, 200, 800 and 2000 rpm.

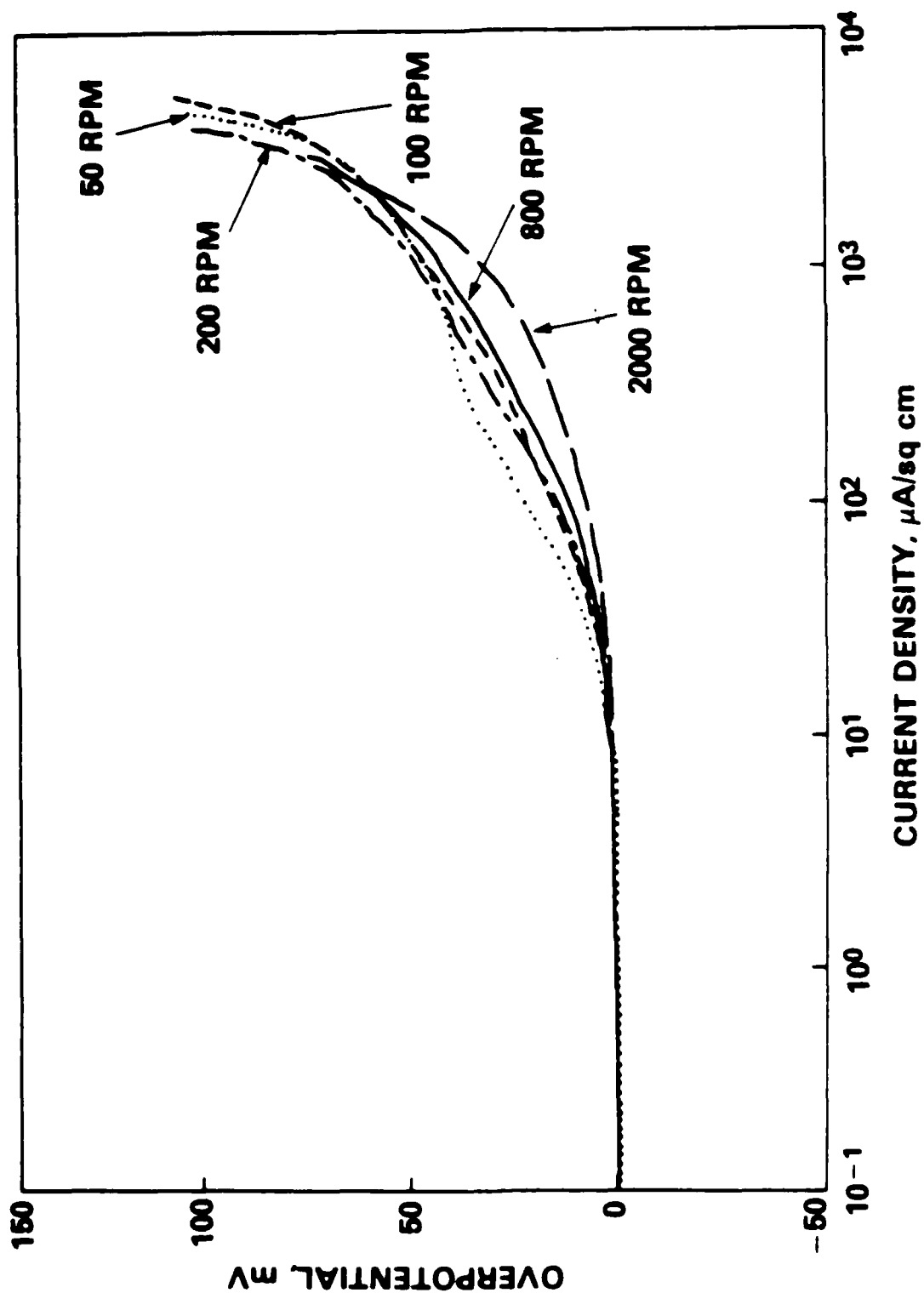


Fig. 7. Plots of polarization curves of zinc anode materials as a function of overpotential.

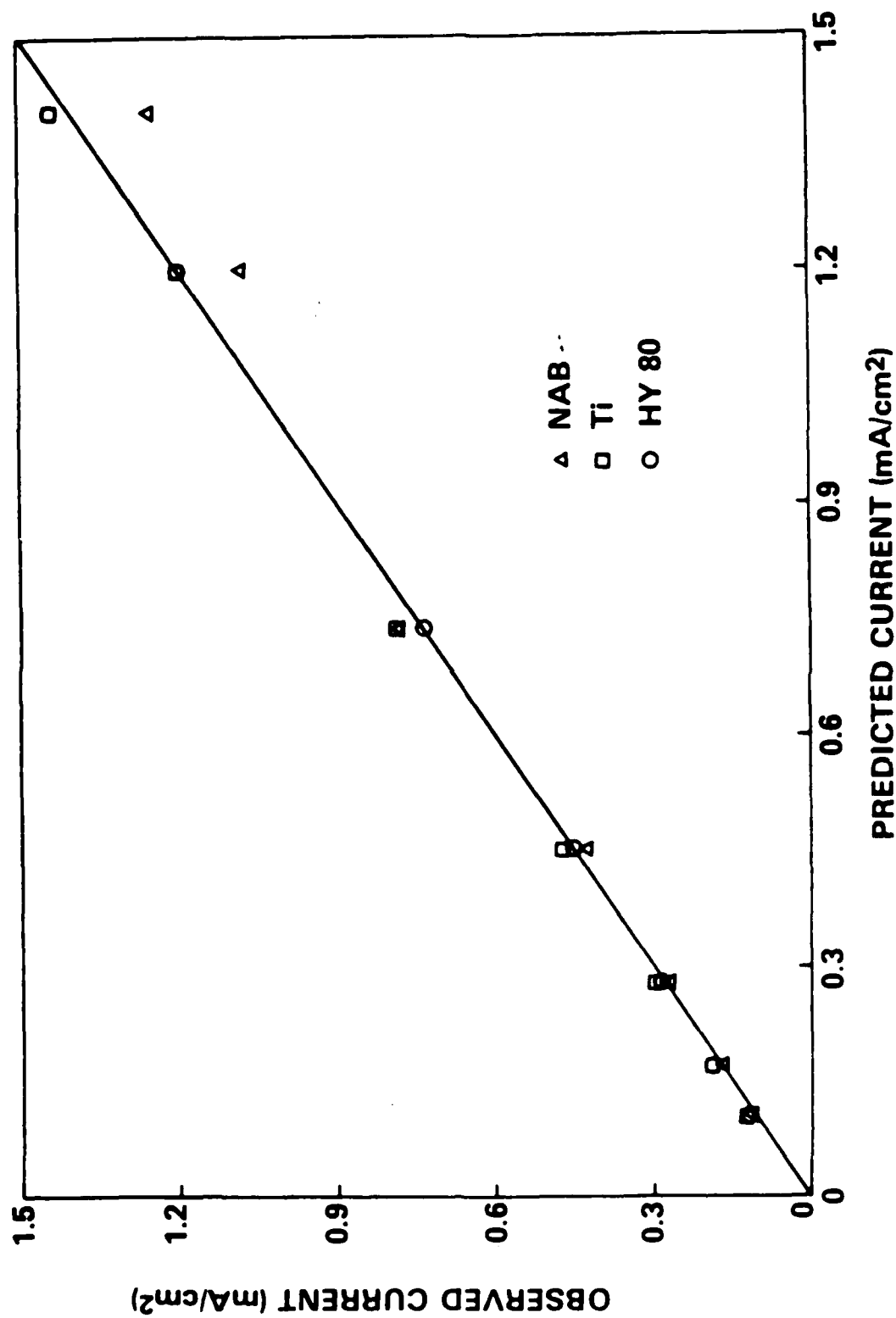


Fig. 8. Comparison of predicted versus observed currents measured by the rotating cylinder electrode apparatus for nickel-aluminum-bronze, CP titanium and HY 80 steel.

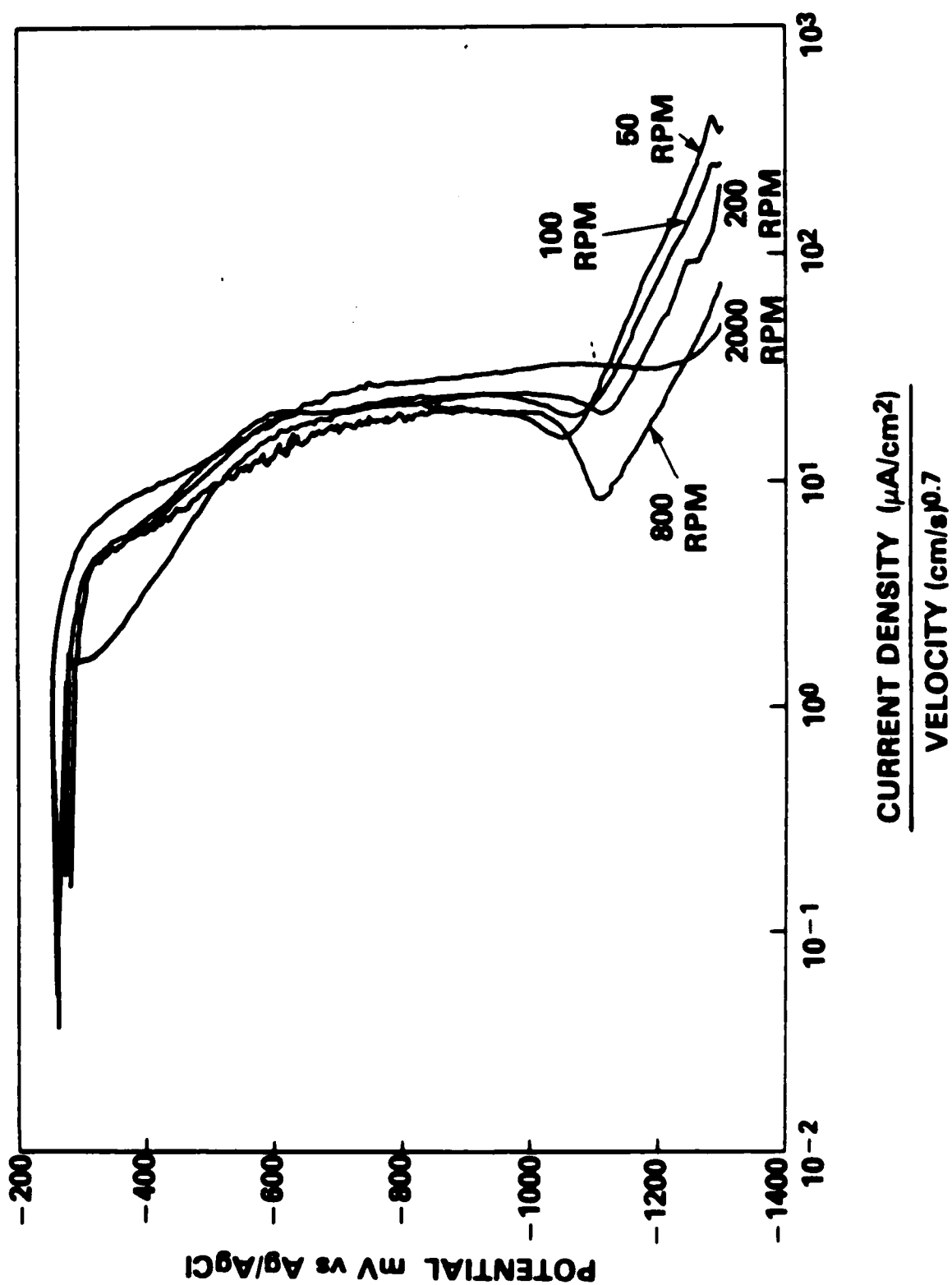


Fig. 9. Normalized polarization curves for nickel-aluminum bronze.

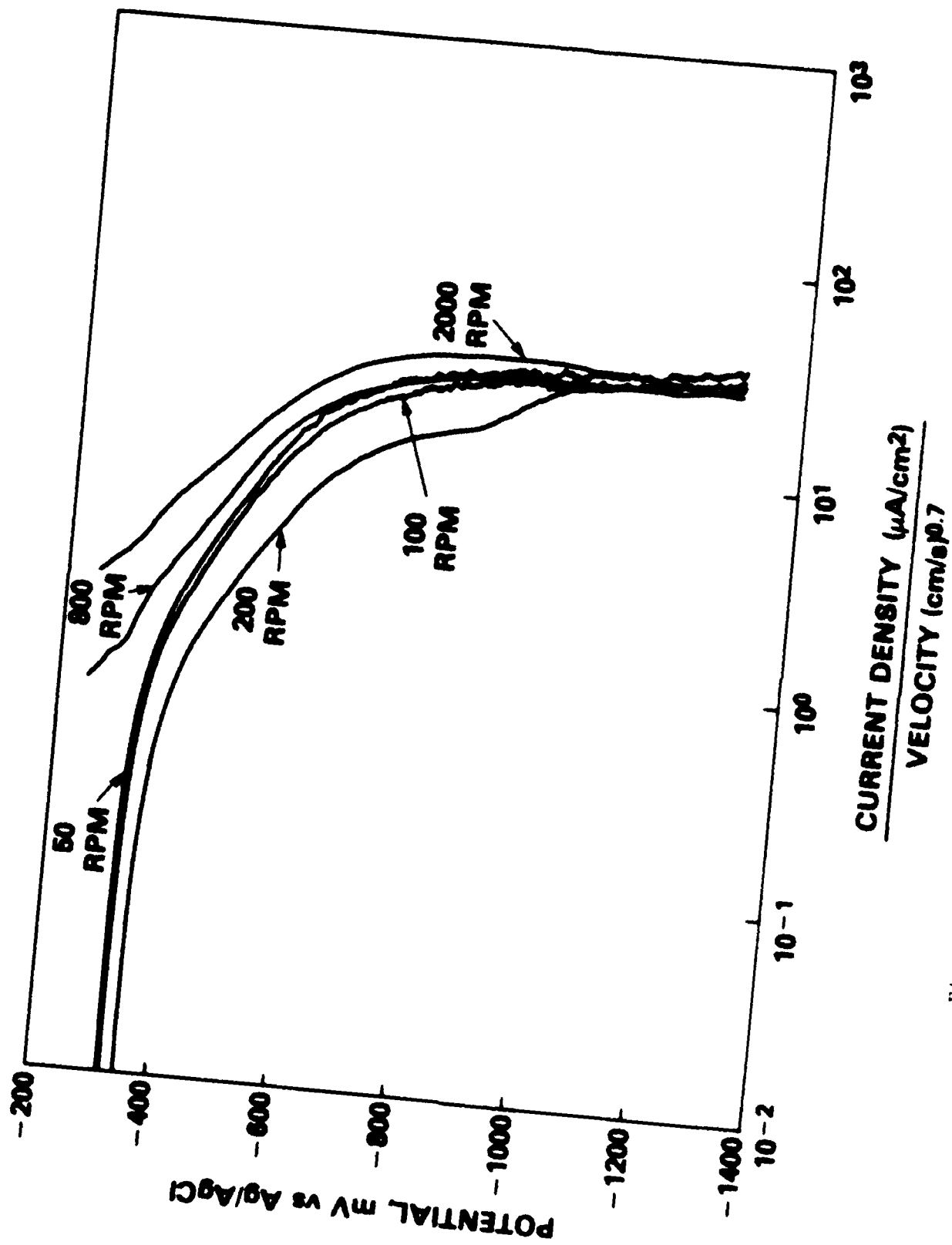


Fig. 10. Normalized polarization curves for CP titanium.

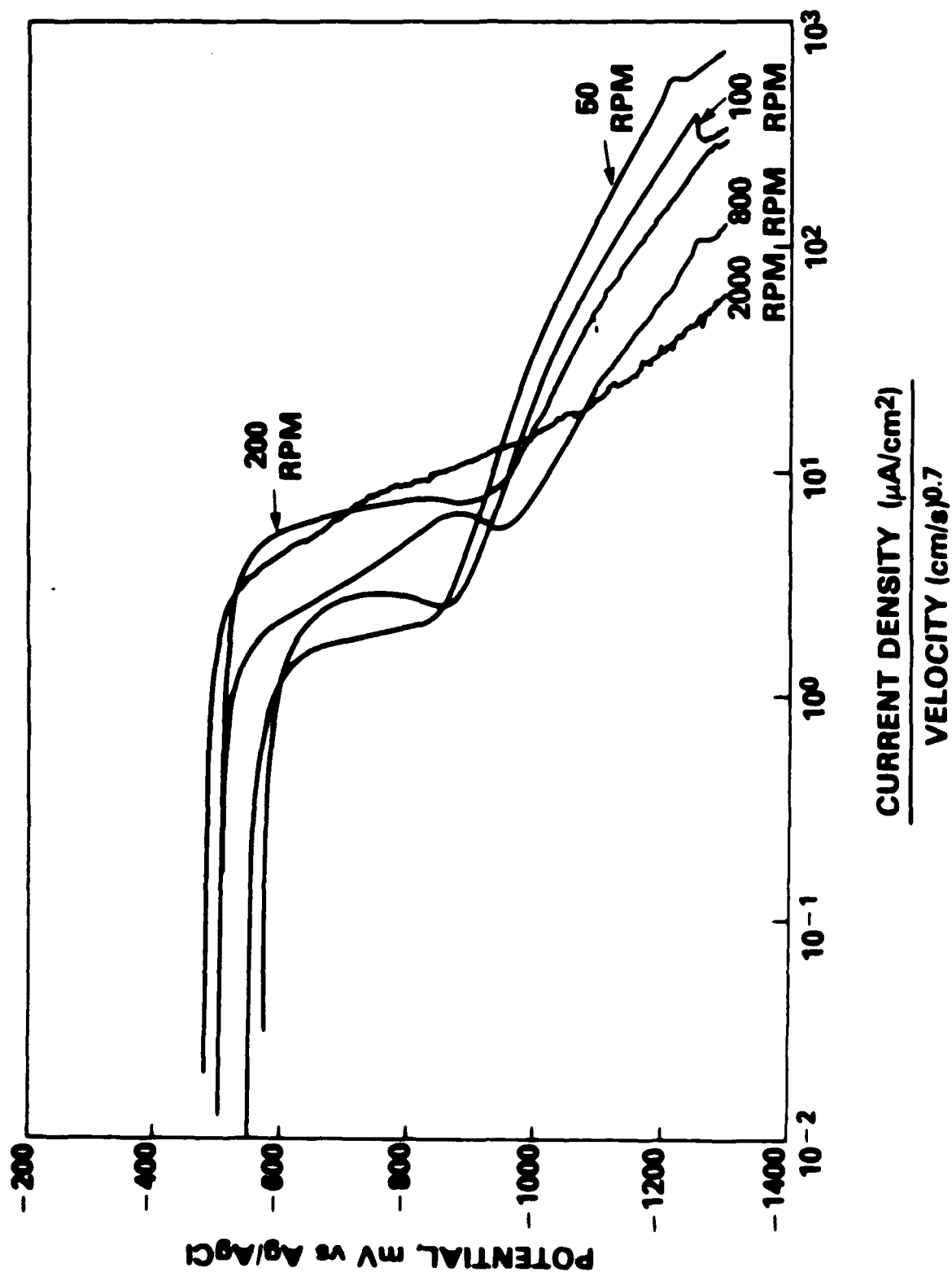


Fig. 11. Normalized polarization curves for HY 80 steel.

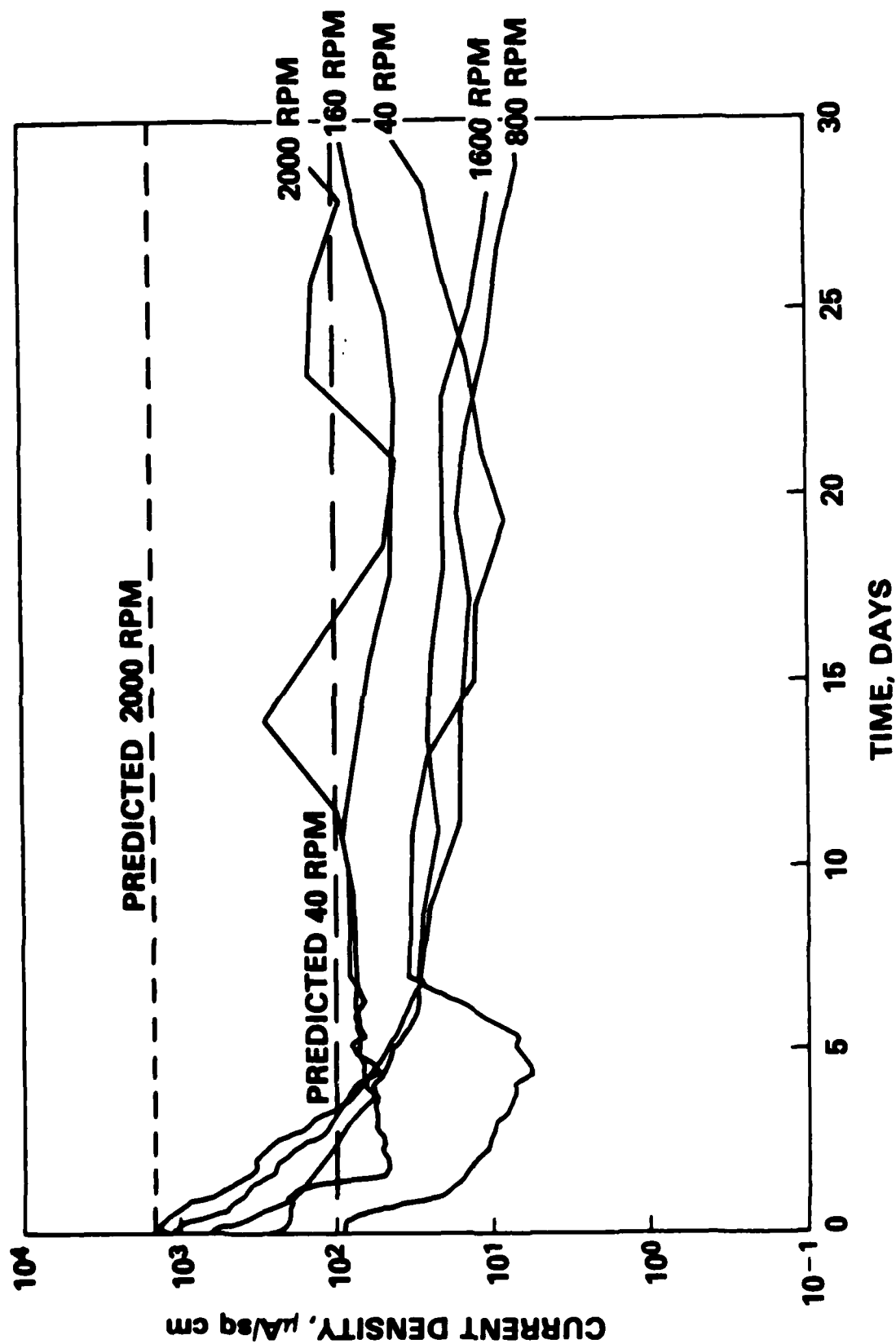


Fig. 12. Long term potentiostatic curves of nickel-aluminum-bronze at 40, 160, 800, 1600 and 2000 rpm.



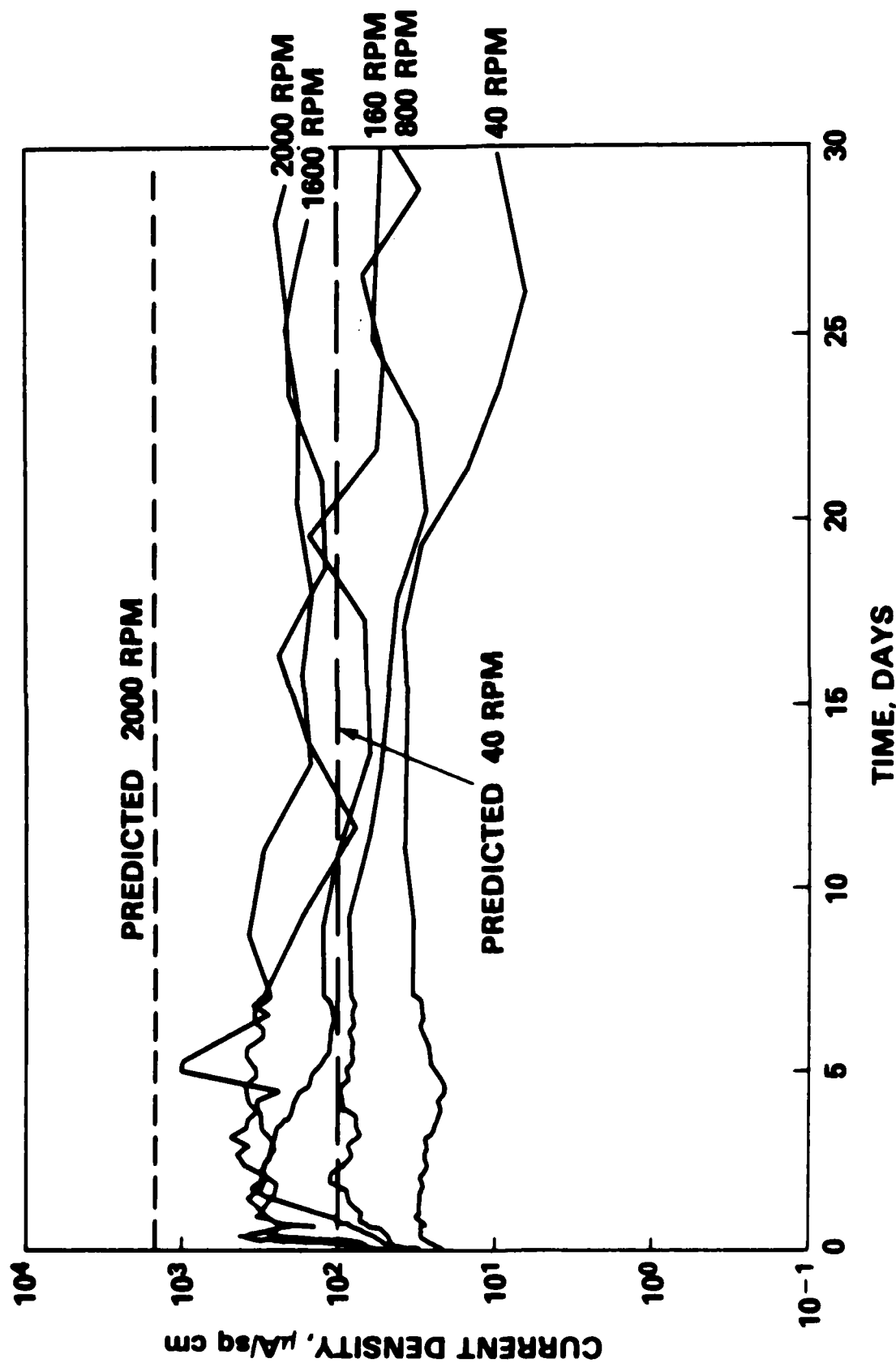


Fig. 13. Long term potentiostatic curves of CP titanium at 40, 160, 800, 1600 and 2000 rpm.

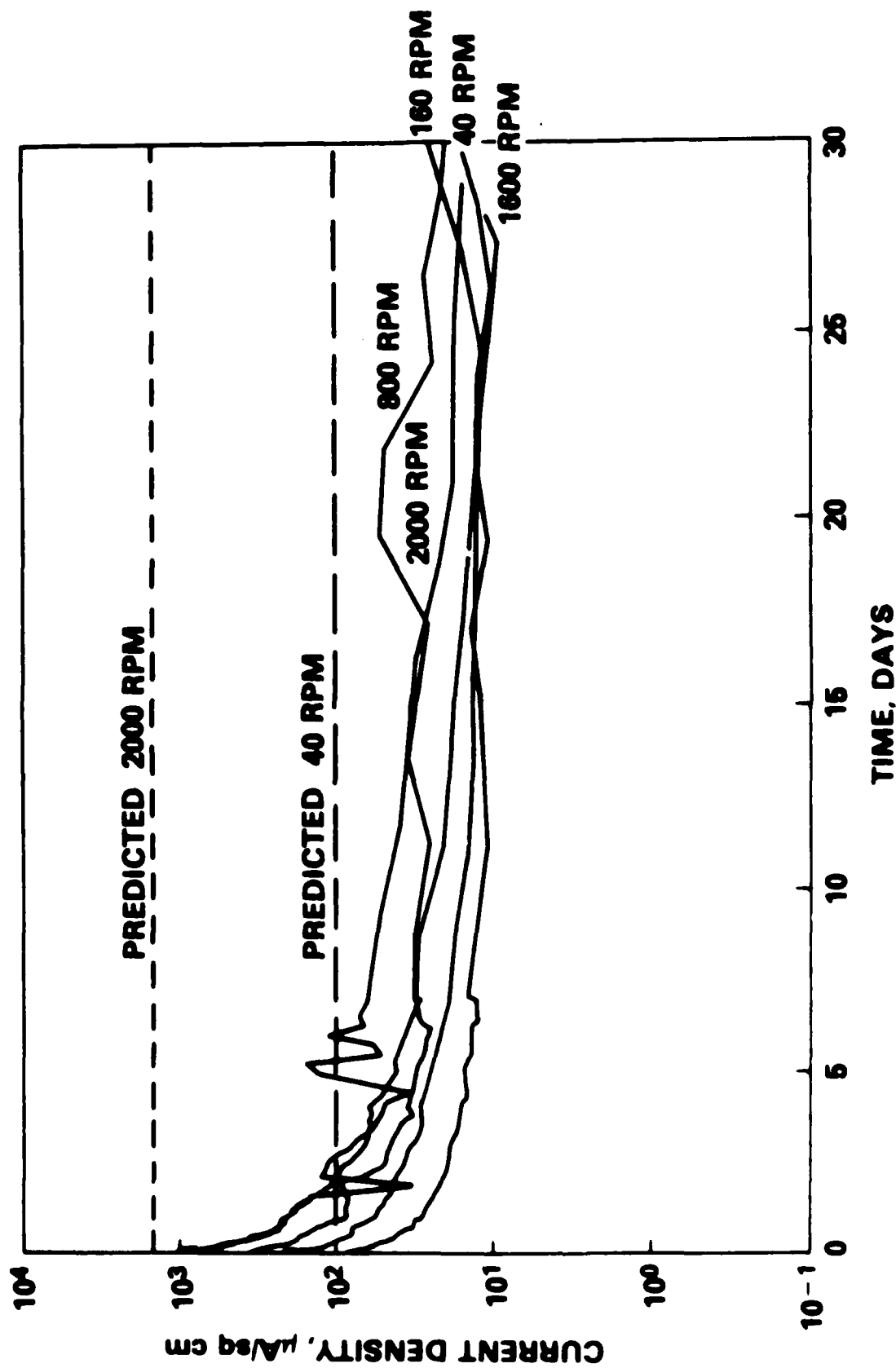



Fig. 14. Long term potentiostatic curves of HY 80 at 40, 160, 800, 1600 and 2000 rpm.

## REFERENCES

1. M. Eisenberg, C.W. Tobias, and C.R. Wilke, J. Electrochem. Soc., Vol. 101, No. 6, (1954).
2. H.P. Hack, "Galvanic Corrosion Prediction Using Long-Term Potentiostatic Polarization Curves," Paper No. 73, Corrosion/83, N.A.C.E., Anaheim, CA, (1983).
3. J.O.M. Bockris, A.K.N. Reddy, Modern Electrochemistry 2, Plenum/ Rosetta, p. 1238, (1977).

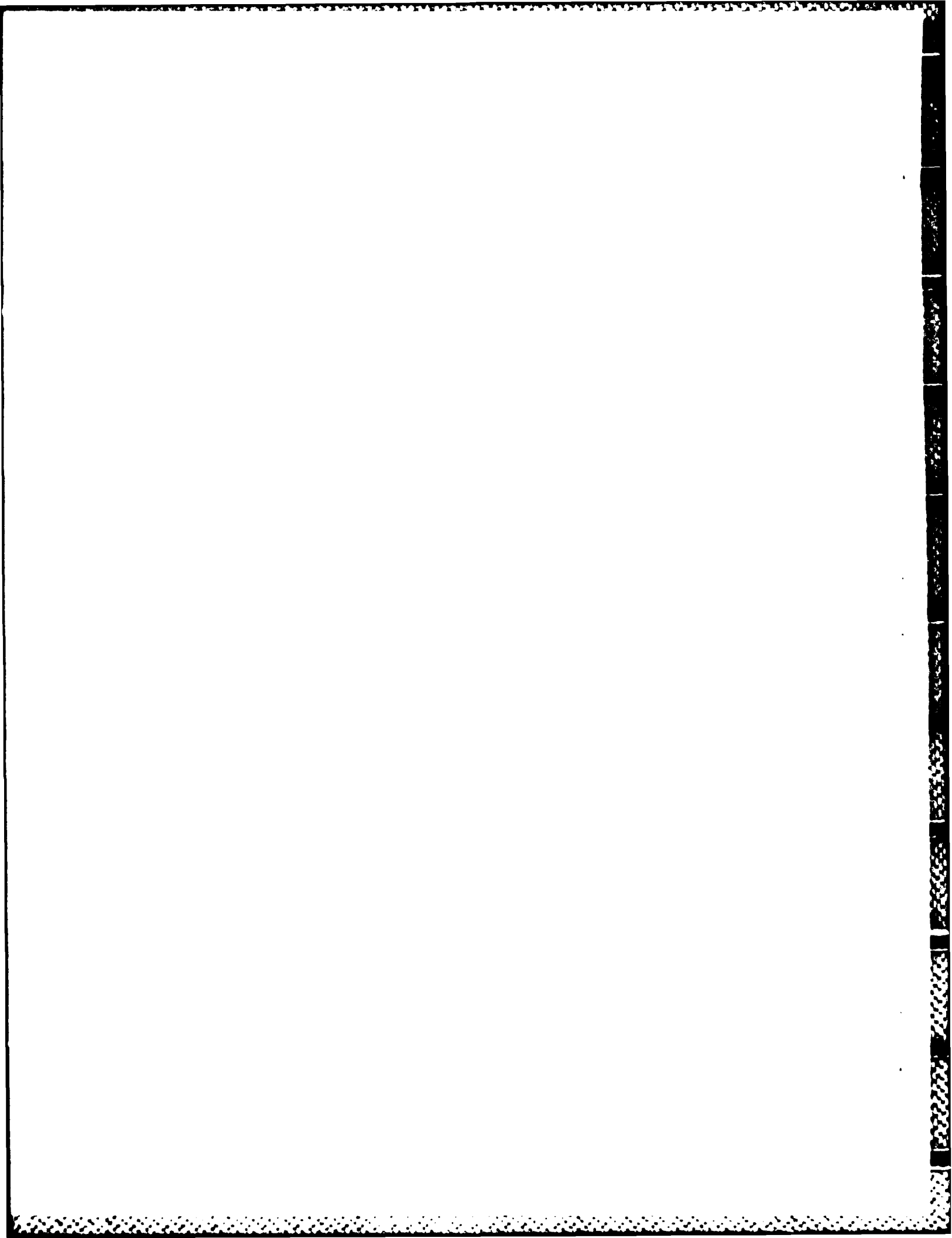
# INITIAL DISTRIBUTION

## Copies

3 NAVSEA  
 1 SEA 05M (Kasnov)  
 1 SEA 56XN3 (Stone)  
 1 SEA 56XN73 (Overway)  
 1 Westinghouse, MTD  
 12 DTIC 

## CENTER DISTRIBUTION

Copies	Code
1	15
3	1508 (Boswell/Howe)
1	1844 (Hurwitz/ Machin)
1	19 (Sevik)
1	1962 (Kilcullen/ Paladino)
1	28
1	2803
1	281
1	2810 (Lengenfelder)
5	2813
10	2813 (Hack)
10	2813 (Guanti)
1	2841
1	522.2 (TIC)
2	5231



### **DTNSRDC ISSUES THREE TYPES OF REPORTS:**

1. **DTNSRDC reports, a formal series**, contain information of permanent technical value. They carry a consecutive numerical identification regardless of their classification or the originating department.
2. **Departmental reports, a semiformal series**, contain information of a preliminary, temporary, or proprietary nature or of limited interest or significance. They carry a departmental alphanumerical identification.
3. **Technical memoranda, an informal series**, contain technical documentation of limited use and interest. They are primarily working papers intended for internal use. They carry an identifying number which indicates their type and the numerical code of the originating department. Any distribution outside DTNSRDC must be approved by the head of the originating department on a case-by-case basis.

END

4-87

DTIC